JCI insight

TECHNICAL ADVANCE

Integrated human pseudoislet system and microfluidic platform demonstrate differences in GPCR signaling in islet cells

John T. Walker,[1] Rachana Haliyur,[1] Heather A. Nelson,[2] Matthew Ishahak,[3] Gregory Poffenberger,[2] Radhika Aramandla,[2] Conrad Reihsmann,[2] Joseph R. Luchsinger,[4] Diane C. Saunders,[2] Peng Wang,[5] Adolfo Garcia-Ocaña,[5] Rita Bottino,[6] Ashutosh Agarwal,[3] Alvin C. Powers,[1,2,7] and Marcela Brissova[2]

[1]Department of Molecular Physiology and Biophysics, Vanderbilt University School of Medicine, Nashville, Tennessee, USA. [2]Division of Diabetes, Endocrinology and Metabolism, Department of Medicine, Vanderbilt University Medical Center, Nashville, Tennessee, USA. [3]Department of Biomedical Engineering, University of Miami, Miami, Florida, USA. [4]Vanderbilt Brain Institute, Vanderbilt University School of Medicine, Nashville, Tennessee, USA. [5]Diabetes, Obesity, and Metabolism Institute, Icahn School of Medicine at Mount Sinai, New York, New York, USA. [6]Institute of Cellular Therapeutics, Allegheny-Singer Research Institute, Allegheny Health Network, Pittsburgh, Pennsylvania, USA. [7]VA Tennessee Valley Healthcare System, Nashville Tennessee, USA.

Pancreatic islets secrete insulin from β cells and glucagon from α cells, and dysregulated secretion of these hormones is a central component of diabetes. Thus, an improved understanding of the pathways governing coordinated β and α cell hormone secretion will provide insight into islet dysfunction in diabetes. However, the 3D multicellular islet architecture, essential for coordinated islet function, presents experimental challenges for mechanistic studies of intracellular signaling pathways in primary islet cells. Here, we developed an integrated approach to study the function of primary human islet cells using genetically modified pseudoislets that resemble native islets across multiple parameters. Further, we developed a microperifusion system that allowed synchronous acquisition of GCaMP6f biosensor signal and hormone secretory profiles. We demonstrate the utility of this experimental approach by studying the effects of G_i and G_q GPCR pathways on insulin and glucagon secretion by expressing the designer receptors exclusively activated by designer drugs (DREADDs) hM4Di or hM3Dq. Activation of G_i signaling reduced insulin and glucagon secretion, while activation of G_q signaling stimulated glucagon secretion but had both stimulatory and inhibitory effects on insulin secretion, which occur through changes in intracellular Ca^{2+}. The experimental approach of combining pseudoislets with a microfluidic system allowed the coregistration of intracellular signaling dynamics and hormone secretion and demonstrated differences in GPCR signaling pathways between human β and α cells.

Authorship note: JTW and RH contributed equally to this work.

Conflict of interest: MI and AA are cofounders of Bio-Vitro, which is in the process of commercializing the microfluidic device.

Submitted: February 5, 2020
Accepted: April 22, 2020
Published: April 30, 2020.

Reference information: *JCI Insight*. 2020;5(10):e137017. https://doi.org/10.1172/jci.insight.137017.

Introduction

Pancreatic islets of Langerhans, small collections of specialized endocrine cells interspersed throughout the pancreas, control glucose homeostasis. Islets are composed primarily of β, α, and δ cells but also include supporting cells, such as endothelial cells, nerve fibers, and immune cells. Insulin, secreted from the β cells, lowers blood glucose by stimulating glucose uptake in peripheral tissues, while glucagon, secreted from α cells, raises blood glucose through its actions in the liver. Importantly, β and/or α cell dysfunction is a key component of all forms of diabetes mellitus (1–11). Thus, an improved understanding of the pathways governing the coordinated hormone secretion in human islets may provide insight into how these may become dysregulated in diabetes.

In β cells, the central pathway of insulin secretion involves glucose entry via glucose transporters where it is metabolized inside the cell, resulting in an increased ATP/ADP ratio. This shift closes ATP-sensitive potassium channels, depolarizing the cell membrane and opening voltage-dependent calcium channels where calcium influx is a trigger of insulin granule exocytosis (12). In α cells, the pathway of glucose inhibition of glucagon secretion is not clearly defined, with both intrinsic and paracrine mechanisms proposed (13–15). Furthermore, gap junctional coupling and paracrine signaling between

islet endocrine cells and within the 3D islet architecture are critical for islet function, as individual α or β cells do not show the same coordinated secretion pattern seen in intact islets (16–20).

The 3D islet architecture, while essential for function, presents experimental challenges for mechanistic studies of intracellular signaling pathways in primary islet cells. Furthermore, human islets show a number of key differences from rodent islets, including their endocrine cell composition and arrangement, glucose set point, and both basal and stimulated insulin and glucagon secretion, highlighting the importance of studying signaling pathways in primary human cells (21–24).

To study signaling pathways in primary human islet cells within the context of their 3D arrangement, we developed an integrated approach that consists of (a) human pseudoislets closely mimicking native human islet biology and allowing for efficient genetic manipulation and (b) a microfluidic system with the synchronous assessment of intracellular signaling dynamics and both insulin and glucagon secretion. Using this experimental approach, we demonstrate differences in G_q and G_i signaling pathways between human β and α cells.

Results

Human pseudoislets resemble native human islets and facilitate virally mediated manipulation of human islet cells. To establish an approach that would allow manipulation of human islets, we adapted a system where in human islets are dispersed into single cells and then reaggregated into pseudoislets (25–29) (Figure 1A and see Vanderbilt Pseudoislet Protocol in Supplemental Information for detailed protocol; supplemental material available online with this article; https://doi.org/10.1172/jci.insight.137017DS1). To optimize the formation and function of human pseudoislets, we investigated two different systems to create pseudoislets, a modified hanging drop system (30, 31) and an ultralow attachment microwell system. We found that both systems generated pseudoislets of comparable quality and function (Supplemental Figure 1, A and B) and thus combined groups for comparisons between native islets and pseudoislets. A key determinant of pseudoislet quality was the use of a nutrient- and growth factor–enriched media (termed Vanderbilt pseudoislet media; see Vanderbilt Pseudoislet Protocol in Supplemental Information for detailed protocol).

Pseudoislet morphology, size, and dithizone (DTZ) uptake resembled that of normal human islets (Figure 1, B–D). Pseudoislet size was controlled to between 150 and 200 μm in diameter by adjusting the seeding cell density and thus resembled the size of an average native human islet. Compared with native islets from the same donor cultured in parallel using the same pseudoislet media, pseudoislets had similar insulin and glucagon content, though insulin content was reduced in pseudoislets from some donors (Figure 1E). Endocrine cell composition was also similar, with the ratio of β, α, and δ cells in pseudoislets unchanged compared with that in cultured native islets from the same donor (Figure 1, F and G).

As the primary function of the pancreatic islet is to sense glucose and other nutrients and dynamically respond with coordinated hormone secretion, we assessed the function of pseudoislets compared with native islets by perifusion. We used the standard perifusion (herein referred to as macroperifusion) approach of the Human Islet Phenotyping Program of the Integrated Islet Distribution Program (IIDP), which has assessed nearly 300 human islet preparations. In this system, approximately 250 islet equivalents (IEQs) are loaded into a chamber and exposed to basal glucose (5.6 mM glucose; white) or various secretagogues (16.7 mM glucose, 16.7 mM glucose and 100 μM isobutylmethylxanthine [IBMX], 1.7 mM glucose and 1 μM epinephrine, 20 mM potassium chloride [KCl]; yellow) (Figure 1H). Pseudoislet insulin secretion was very similar to that of native islets in biphasic response to glucose, cAMP-evoked potentiation, epinephrine-mediated inhibition, and KCl-mediated depolarization (Figure 1H). Pseudoislets and native islets also had comparable glucagon secretion, which was inhibited by high glucose and stimulated by cAMP-mediated processes (IBMX and epinephrine) and depolarization (KCl) (Figure 1I). Compared with native islets on the day of arrival, pseudoislets largely maintained both insulin and glucagon secretion after 6 days of culture, with the exception of a slightly diminished second-phase glucose-stimulated insulin secretion and an enhanced glucagon response to epinephrine in cultured native islets and pseudoislets (Supplemental Figure 1, C–N). These results demonstrate that, after dispersion into the single-cell state, human islet cells can reassemble and reestablish intraislet connections crucial for coordinated hormone release across multiple signaling pathways.

Interestingly, the islet architecture of both native whole islets and pseudoislets cultured for 6 days showed β cells primarily on the islet periphery, with α cells and δ cells situated within an interior layer. Furthermore, the core of both the cultured native islets and pseudoislets consisted largely of extracellular

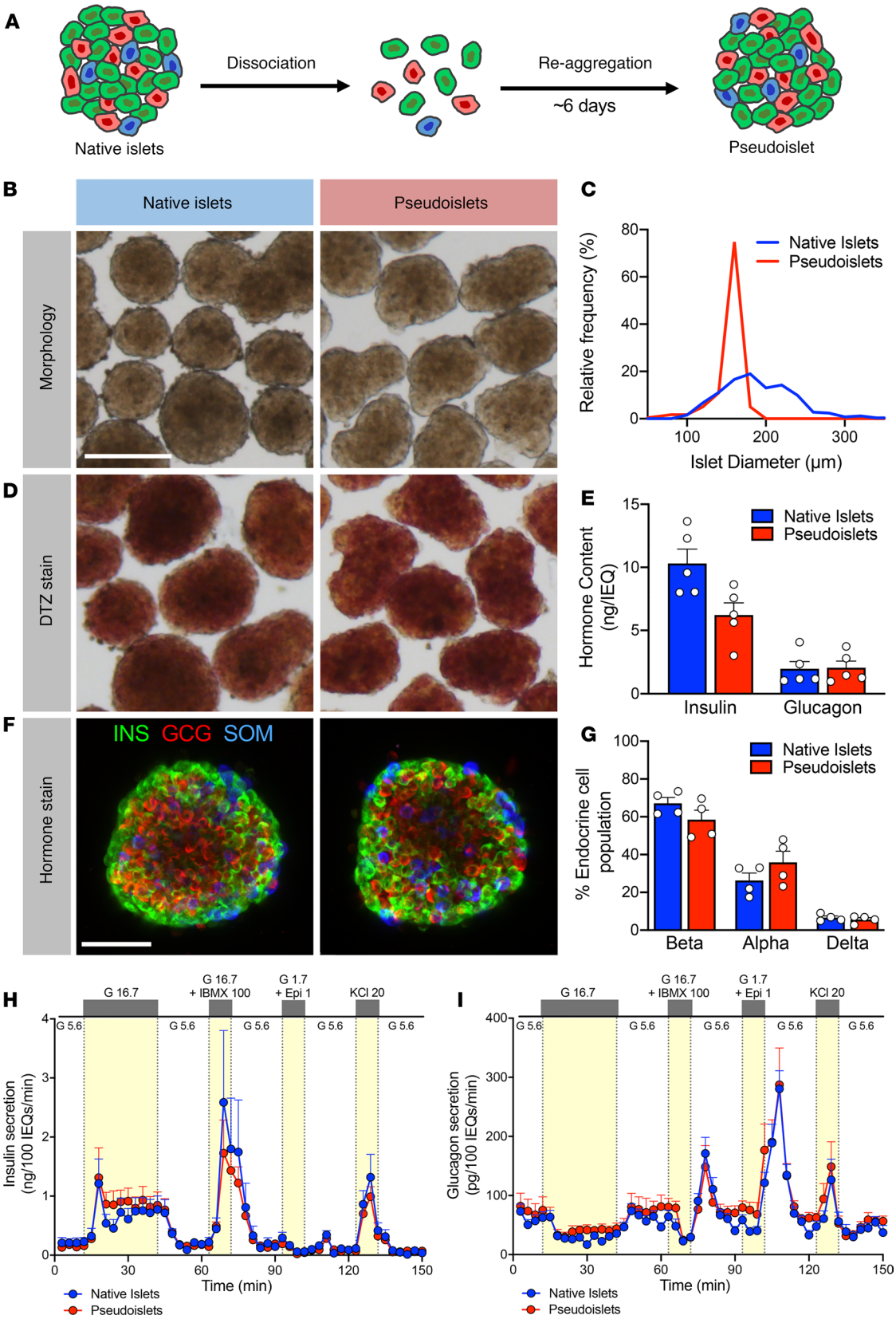

Figure 1. Pseudoislets resemble native human islets in morphology, cell composition, and function. (**A**) Schematic of pseudoislet formation. (**B**) Bright-field images showing the morphology of native islets and pseudoislets. Scale bar: 200 μm. (**C**) Relative frequency plot of islet diameter comparing hand-picked native islets with pseudoislets from the same donor. (**D**) Dithizone (DTZ) uptake of native islets and pseudoislets. Scale bar: 200 μm. (**E**) Insulin and glucagon content normalized to islet volume expressed in islet equivalents (IEQs); 1 IEQ corresponds to an islet with a diameter of 150 μm; n = 5 donors; $P > 0.05$. (**F**) Confocal images of native islets and pseudoislets stained for insulin (INS; β cells), glucagon (GCG; α cells),

and somatostatin (SOM; δ cells). Scale bar: 50 μm. (**G**) Quantification of relative endocrine cell composition of native islets and pseudoislets; $n = 4$ donors; $P > 0.05$. Insulin (**H**) and glucagon (**I**) secretory response to various secretagogues measured by perifusion of native islets and pseudoislets from the same donor ($n = 5$). G 5.6, 5.6 mM glucose; G 16.7, 16.7 mM glucose; G 16.7 + IBMX 100, 16.7 mM glucose with 100 μM isobutylmethylxanthine (IBMX); G1.7 + Epi 1, 1.7 mM glucose and 1 μM epinephrine; KCl 20, 20 mM potassium chloride (KCl). Wilcoxon matched-pairs signed-rank test was used to analyze statistical significance in **E** and **G**. **H** and **I** were analyzed by 2-way ANOVA; $P > 0.05$. The area under the curve for each secretagogue was compared by 1-way ANOVA with Dunn's multiple comparison test (Supplemental Figure 1, E–H and J–M). Data are represented as mean ± SEM.

matrix (collagen IV) and endothelial cells (caveolin-1) (Figure 2, A–C), likely reflective of the consequences of culture and the loss of shear stress along endothelial cells. The survival of intraislet endothelial cells in culture for an extended period of time could be due to the nutrient- and growth factor–enriched media. Additionally, the islet cell arrangement suggests that extracellular matrix and endothelial cells may facilitate pseudoislet assembly. Proliferation, as assessed by Ki67, was low in both native and pseudoislets, with β cells below 0.5% and α cells around 1% (Figure 2, A and D). Similarly, apoptosis, as assessed by TUNEL, was very low (<0.5%) in pseudoislets and cultured human islets (Figure 2, A and E). Interestingly, endothelial cells appear to have greater turnover, as evidenced by the presence of both Ki67 and TUNEL staining in the core of both native islets and pseudoislets (Figure 2A).

To assess markers of α and β cell identity in pseudoislets, we investigated expression of several key islet-enriched transcription factors. The expression of β (PDX1, NKX6.1) and α cell markers (MAFB, ARX) as well as those expressed in both cell types (PAX6, NKX2.2) was maintained in pseudoislets when compared with native islets (Figure 2, F–J), indicating that the process of dispersion and reaggregation does not affect islet cell identity.

The 3D structure of intact islets makes virally mediated manipulation of human islet cells challenging due to poor viral penetration into the center of the islet. We adopted the pseudoislet system to overcome this challenge by transducing the dispersed single islet cells before reaggregation (Figure 3A). To optimize transduction efficiency and subsequent pseudoislet formation, we incubated with adenovirus for 2 hours in Vanderbilt pseudoislet media at a multiplicity of infection of 500. Transducing pseudoislets with control adenovirus did not affect pseudoislet morphology or function and achieved high transduction efficiency of β and α cells throughout the entire pseudoislet (Supplemental Figure 2, A–E). Interestingly, β cells showed a higher transduction efficiency (90%) than α cells (70%), suggesting that α cells may be inherently more difficult to transduce with adenovirus (Supplemental Figure 2B).

Activation of G_i signaling reduces insulin and glucagon secretion. To investigate the value of this experimental approach, we sought to perturb islet gene expression and then assess islet cell function. We chose to alter GPCR signaling in islet cells because GPCRs are known to modulate islet hormone secretion (32, 33). GPCRs, a broad class of integral membrane proteins, mediate extracellular messages to intracellular signaling through activation of heterotrimeric G proteins, which can be broadly classified into distinct families based on the G_α subunit, including G_i-coupled and G_q-coupled GPCRs (34). An estimated 30%–50% of clinically approved drugs target or signal through GPCRs, including multiple used for diabetes treatment (35, 36).

Studying GPCR signaling with endogenous receptors and ligands can be complicated by a lack of specificity — ligands that can activate multiple receptors or receptors that can be activated by multiple ligands. To overcome these limitations, we used the DREADD technology (37). DREADDs are GPCRs with specific point mutations that render them unresponsive to their endogenous ligand. Instead, they can be selectively activated by the otherwise inert ligand, clozapine-N-oxide (CNO), thus providing a selective and inducible model of GPCR signaling (37, 38). DREADDs are commonly used in neuroscience as molecular switches to activate or repress neurons with G_q or G_i signaling, respectively (39). In contrast, there have been comparatively very few studies using DREADDs in the field of metabolism, but there have been investigations of the G_q and G_s DREADD in mouse β cells and the G_i DREADD in mouse α cells (16, 40). The G_s-coupled DREADD has been reported to be leaky and have basal activation, and thus, we chose here to focus on the 2 most commonly used DREADDs, G_i and G_q, to demonstrate how this experimental approach can be used. To our knowledge this is the first study to use this powerful technology in human islets.

To investigate G_i-coupled GPCR signaling, we introduced adenovirus encoding hM4Di (Ad-CMV-hM4Di-mCherry), a G_i DREADD, into dispersed human islet cells, allowed reaggregation into pseudoislets and then tested the effect of activated G_i signaling (Figure 3A). G_i-coupled GPCRs signal by inhibiting adenylyl cyclase, thus reducing cAMP, and by activating inwardly rectifying potassium channels (Figure 3B).

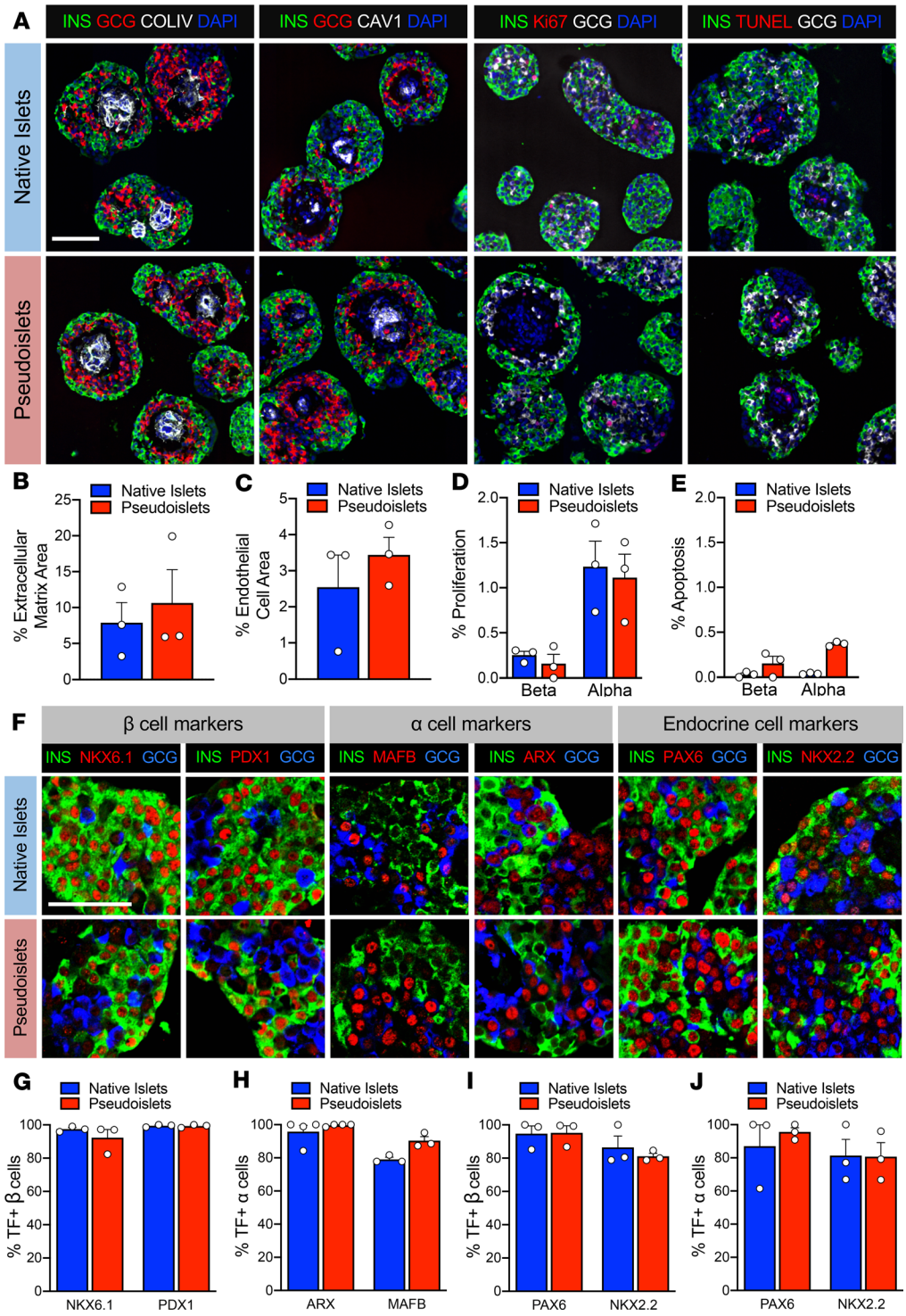

Figure 2. Pseudoislets resemble native human islets in proliferation, apoptosis, and architecture and express markers of α and β cell identity. (**A**) Immunofluorescence visualization of labeling for insulin (INS; β cells) and glucagon (GCG; α cells) in combination with detection of proliferation (Ki67), apoptosis (TUNEL), extracellular matrix (collagen IV, COLIV), and endothelial cells (caveolin-1, CAV1). Scale bar: 100 μm. (**B**) Quantification of β and α cell proliferation in native islets and pseudoislets, expressed as a percentage of INS$^+$ or GCG$^+$ cells expressing Ki67; n = 3 donors; $P > 0.05$. (**C**) Quantification of β and α cell apoptosis by TUNEL assay; n = 3 donors; $P > 0.05$. (**D**) Quantification of COLIV-expressing extracellular matrix, expressed as percentage of COLIV$^+$ area to INS$^+$ and GCG$^+$ cell area; n = 3 donors; $P > 0.05$. (**E**) Quantification of endothelial cell area, expressed as percentage of CAV1$^+$ cell area to INS$^+$ and GCG$^+$ cell area; n = 3 donors; $P > 0.05$. (**F**) Expression of transcription factors (TF) important for β cell identity (NKX6.1 and PDX1), α cell identity (MAFB and ARX), and pan endocrine cell identity (PAX6 and NKX2.2). Scale bar: 50 μm. (**G**) Quantification β cell identity markers in β cells of native islets and pseudoislets (n = 3 donors/marker; $P > 0.05$). (**H**) Quantification of α cell identity markers in α cells of native islets and pseudoislets (n = 3–4 donors/marker; $P > 0.05$). (**I** and **J**) Quantification of pan-endocrine markers in β (**I**) and α (**J**) cells of native islets and pseudoislets (n = 3 donors/marker; $P > 0.05$). Wilcoxon matched-pairs signed-rank test was used to analyze statistical significance in **B–E** and **G–J**. Data are represented as mean ± SEM.

Endogenous GPCRs, which couple to G_i proteins, include the somatostatin receptor in all islet cells as well as the α_2 adrenergic receptor in β cells (32, 33). CNO (10 μM) had no effect on insulin or glucagon secretion in mCherry-expressing pseudoislets (Supplemental Figure 2, F and G), thus we compared the dynamic hormone secretion of hM4Di-expressing pseudoislets with and without CNO in response to a glucose ramp (2 mM glucose, 7 mM glucose, 11 mM glucose, 20 mM glucose; gray) and depolarization by KCl (20 mM; yellow) by perifusion (Figure 3, C and G). Activation of G_i signaling had clear inhibitory effects on insulin secretion by β cells at low glucose, which became more prominent with progressively higher glucose concentrations (gray shading; Figure 3, C–E). Furthermore, bypassing glucose metabolism

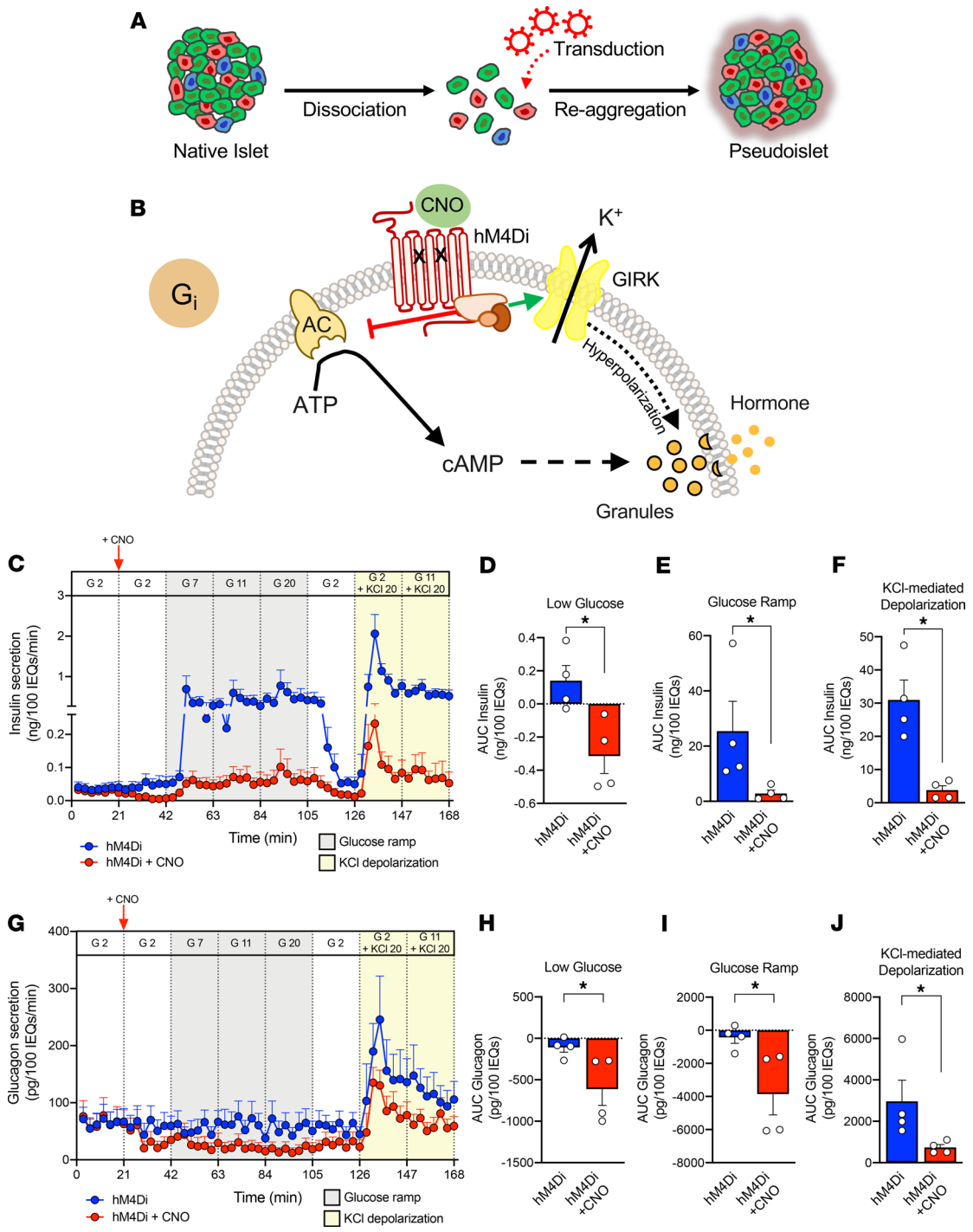

Figure 3. G_i activation reduces insulin and glucagon secretion. (**A**) Schematic of incorporation of efficient viral transduction into pseudoislet approach. (**B**) Schematic of the G_i-coupled GPCR signaling pathway. CNO, clozapine-N-oxide; AC, adenylyl cyclase; ATP, adenosine triphosphate; GIRK, G protein–coupled inwardly rectifying potassium channel; K^+, potassium ion. (**C**) Dynamic insulin secretion assessed by macroperifusion in response to low glucose (G 2, 2 mM glucose; white), glucose ramp (G 7, 7 mM; G 11, 11 mM; G 20, 20 mM glucose; gray), and KCl-mediated depolarization (KCl 20, 20 mM potassium chloride in the presence of G 2 or G 11; yellow) in the absence (blue trace) or presence of CNO (red trace); n = 4 donors/each. 10 μM CNO was added after the first period of 2 mM glucose, as indicated by a vertical red arrow and then continuously administered for the duration of the experiment (red trace). Note the split of y axis to visualize differences between traces at G 2 ± CNO. (**D–F**) Insulin secretion was integrated by calculating the area under the curve (AUC) for response to the low glucose (white), glucose ramp (gray), and KCl-mediated depolarization (yellow). Baseline was set to the average value of each trace from 0 to 21 minutes (before CNO addition). (**G–J**) Glucagon secretion was analyzed in parallel with insulin as described above. Insulin and glucagon secretory traces in **C** and **G**, respectively, were compared in the absence versus presence of CNO by 2-way ANOVA; $^{****}P < 0.0001$ for both insulin and glucagon secretion. Area under the curve of insulin (**D–F**) and glucagon responses (**H–J**) to low glucose, glucose ramp, and KCl-mediated depolarization were compared in the absence versus presence of CNO by Mann-Whitney test; $^*P < 0.05$. Data are represented as mean ± SEM.

by directly activating β cells via depolarization with potassium chloride did not overcome this inhibition by G_i signaling (yellow shading; Figure 3, C and F). Together, these data demonstrate that in human β cells G_i signaling significantly attenuates, but does not completely prevent, insulin secretion and that this effect, at least in part, occurs downstream of glucose metabolism.

The activation of G_i signaling also had inhibitory effects on glucagon secretion (Figure 3, G–J). We did not observe a substantial inhibition of glucagon secretion in the hM4Di and hM4Di+CNO group in response to glucose, but activation of G_i signaling with CNO caused a clear reduction in glucagon secretion, and secretion remained lower in the hM4Di+CNO group than in control hM4Di pseudoislets. When stimulated with potassium chloride, pseudoislets with activated G_i signaling increased glucagon secretion but not to the level of controls. This demonstrates that the inhibitory effects of G_i signaling persist even if the α cell is directly activated by depolarization. Thus, in α cells, activation of G_i signaling reduces glucagon secretion across a range of glucose levels and when the cell is depolarized by potassium chloride.

Activation of G_q signaling greatly stimulates glucagon and somatostatin secretion but has both stimulatory and inhibitory effects on insulin secretion. G_q-coupled GPCRs signal through phospholipase C, leading to IP_3-mediated Ca^{2+} release from the endoplasmic reticulum (Figure 4A). Endogenous GPCRs, which couple to G_q proteins in islets, include the M_3 muscarinic receptor and the free fatty acid receptor FFAR (also known as GPR40) (32, 33). To investigate G_q-coupled GPCR signaling, we introduced hM3Dq (Ad-CMV-hM3Dq-mCherry), a G_q DREADD, into dispersed human islet cells, allowed reaggregation, and assessed hM3Dq-expressing pseudoislets by perifusion. When CNO was added to activate G_q signaling, there was an acute increase in insulin secretion. However, this was not sustained, as insulin secretion fell quickly back to baseline, highlighting a dynamic response to G_q signaling in β cells (Figure 4, B–E). Furthermore, continued G_q activation inhibited glucose-stimulated insulin secretion, suggesting that in certain scenarios G_q signaling may override the ability of glucose to stimulate insulin secretion. These results highlight the value of assessing hormone secretion in the dynamic perifusion system. Finally, G_q activation reduced, but did not completely prevent, insulin secretion in response to direct depolarization with potassium chloride, indicating that the inhibitory effects cannot be overcome by bypassing glucose metabolism and suggesting that they occur downstream of the K_{ATP} channel. Together, these data indicate that activated G_q signaling can have both stimulatory and inhibitory effects on human β cells.

In contrast, activation of G_q signaling in α cells robustly increased glucagon secretion in low glucose, and it remained elevated with continued CNO exposure during glucose ramp as well as in the presence of potassium chloride (Figure 4, F–I). This indicates that in contrast to the β cells, activation of G_q signaling in α cells robustly stimulates glucagon secretion, and this response is sustained across a glucose ramp and during KCl-mediated depolarization.

Given the differing responses in β and α cells and the potential for paracrine signaling, we sought to measure somatostatin secretion and elucidate the effect of G_q activation in δ cells. The relatively low abundance of δ cells in the native islets and pseudoislets (approximately 5%) prevented detection of somatostatin in the perifusion and microperifusion experiments (below assay sensitivity), so we tested the effect of CNO in low (2 mM) and high (11 mM) glucose in the context of static incubation. In glucose alone, somatostatin secretion was below the assay detection limit in 3 of the 4 donors tested; in contrast, activation of G_q signaling increased somatostatin secretion in both low and high glucose (Supplemental Figure 3, A–D), showing that G_q signaling robustly stimulates δ cells.

Integration of the pseudoislet system with genetically encoded biosensor and microfluidic device allows synchronous measurement of intracellular signals and hormone secretion. While conventional macroperifusion systems, including the perifusion system used in this study, reliably assess islet hormone secretory profiles (3, 6, 7, 41, 42), their configuration does not allow coupling with imaging systems to measure intracellular signaling. To overcome this challenge, we developed an integrated microperifusion system consisting of pseudoislets and a microfluidic device that enables studies of islet intracellular signaling using genetically encoded biosensors in conjunction with hormone secretion (Figure 5A and Supplemental Figure 4, A–C). The microfluidic device (Supplemental Figure 4A) (43) is made of bioinert and nonabsorbent materials, with optimized design for nutrient delivery, synchronous islet imaging by confocal microscopy, and collection of effluent fractions for analysis of insulin and glucagon secretion. The microperifusion system uses smaller volumes, slower flow rates, and fewer islets than our conventional macroperifusion system (Supplemental Figure 4, D–F).

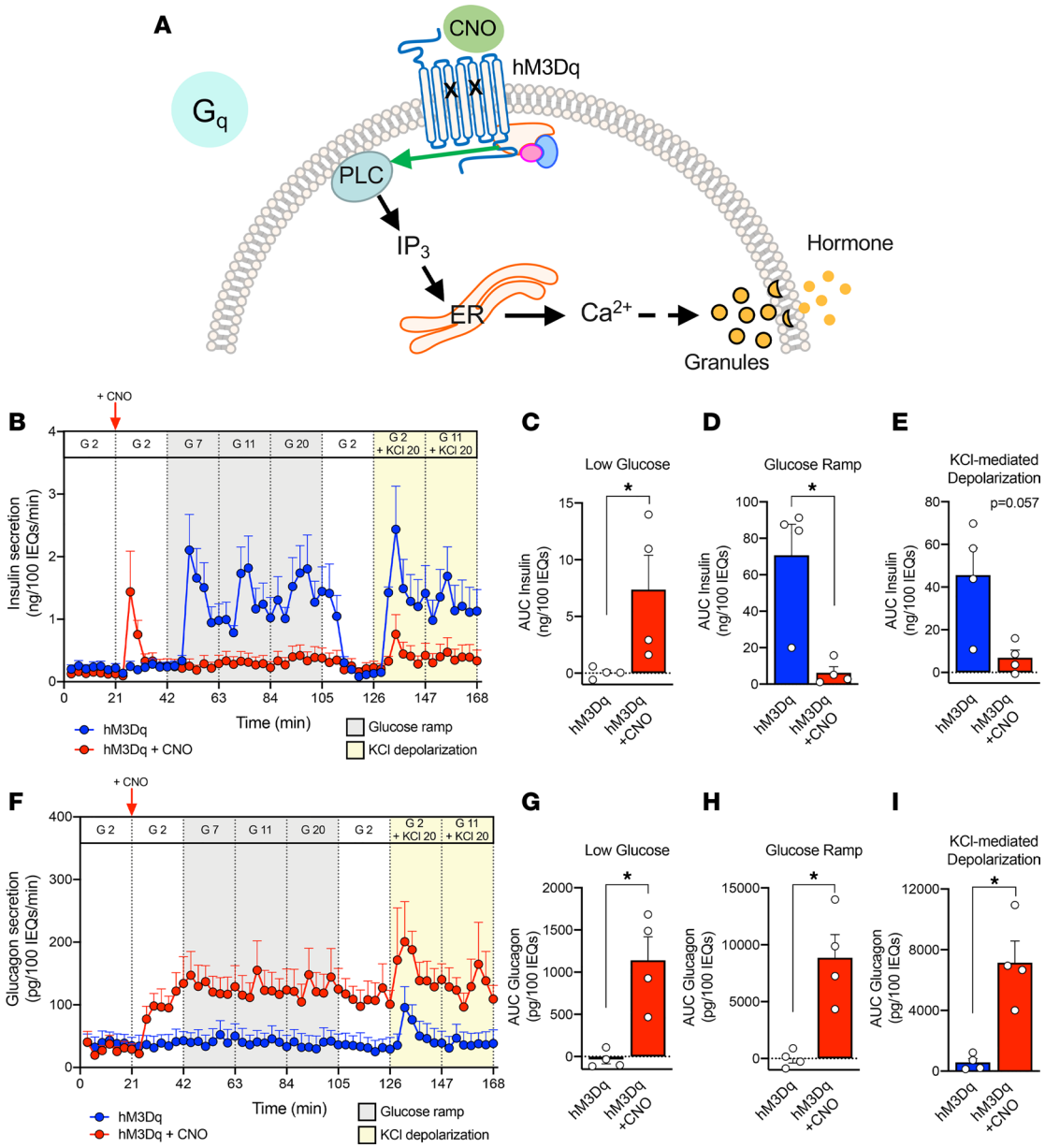

Figure 4. G_q activation stimulates glucagon secretion but has stimulatory and inhibitory effects on insulin secretion. (**A**) Schematic of the G_q-coupled GPCR signaling pathway. CNO, clozapine-N-oxide; PLC, phospholipase C; IP_3, inositol triphosphate; ER, endoplasmic reticulum; Ca^{2+}, calcium ion. (**B–E**) Dynamic insulin secretion was assessed by macroperifusion and analyzed, as described in detail in Figure 3; n = 4 donors/each. (**F–I**) Glucagon secretion was analyzed in parallel with insulin, as described in Figure 3. Insulin and glucagon secretory traces in **B** and **F**, respectively, were compared in the absence versus presence of CNO by 2-way ANOVA; $^{****}P < 0.0001$ for both insulin and glucagon secretion. Area under the curve of insulin (**C–E**) and glucagon responses (**G–I**) to each stimulus were compared in the absence versus presence of CNO by Mann-Whitney test; $^{*}P < 0.05$. Data are represented as mean ± SEM.

To investigate the dual effects of activated G_q signaling on insulin secretion, we cotransduced pseudoislets with hM3Dq and GCaMP6f (Supplemental Figure 4C), a calcium biosensor (Ad-CMV-GCaMP6f), as the G_q pathway conventionally signals through intracellular Ca^{2+} (Figure 4A). In the absence of CNO, hM3Dq-expressing pseudoislets had stepwise increases in GCaMP6f relative intensity as glucose increased, corresponding to increasing intracellular Ca^{2+} and highlighting the added value of the system (Figure 5B). This intracellular Ca^{2+} response to stepwise glucose increase was accompanied by increasing insulin secretion (Figure 5C), but the first phase of insulin secretion was not as clearly resolved as in the macroperifusion (Figure 4B).

Since there are differences in the design of the macroperifusion and microperifusion systems, we used multiphysics computational modeling with finite element analysis (44, 45) to model the insulin secretion dynamics of the two systems (Supplemental Figure 4, H and I). This modeling accurately predicted the

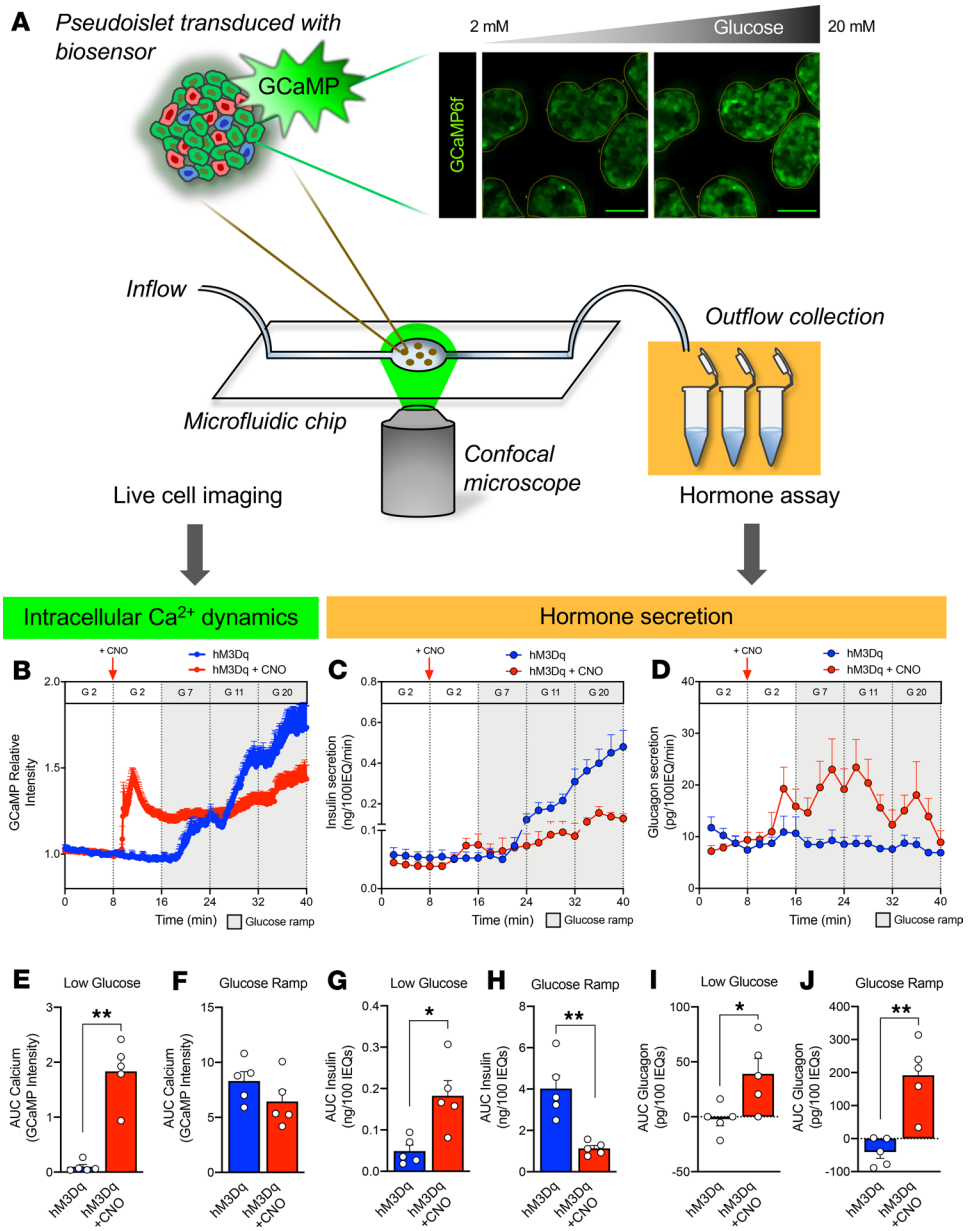

Figure 5. Pseudoislet system integrated with microfluidic device allows for coregistration of hormone secretion and intracellular signaling dynamics. (**A**) Schematic of pseudoislet system integration with a microfluidic device to allow for synchronous detection of intracellular signaling dynamics by the genetically encoded GCaMP6f biosensor and confocal microscopy and collection of microperifusion efflux for hormone analysis. Dynamic changes in GCaMP6f relative intensity (**B**), insulin secretion (**C**), and glucagon secretion (**D**) assessed during microperifusion in response to a low glucose (G 2 – 2 mM glucose; white), glucose ramp (G 7, 7 mM; G 11, 11 mM; and G 20, 20 mM glucose; gray) and in the absence (blue trace) or presence of CNO (red trace); n = 3 donors/each. 10 μM CNO was added after the first period of 2 mM glucose, as indicated by a vertical red arrow and then continuously administered for the duration of the experiment (red trace). See Supplemental Videos 1 and 2 for representative visualization of each experiment. Calcium signal (**E** and **F**) and insulin (**G** and **H**) and glucagon (**I** and **J**) secretion was integrated by calculating the area under the curve (AUC) for response to the low glucose (white) and glucose ramp (gray). Baseline was set to the average value of each trace from 0 to 8 minutes (before CNO addition). Calcium and hormone traces in **B**–**D** were compared in the absence versus presence of CNO by 2-way ANOVA; $^{*}P < 0.05$ for calcium trace, $^{****}P < 0.0001$ for both insulin and glucagon secretion. Area under the curve of calcium (**E** and **F**), insulin (**G** and **H**), and glucagon responses (**I** and **J**) to low glucose and glucose ramp were compared in the absence versus presence of CNO by Mann-Whitney test; $^{*}P < 0.05$, $^{**}P < 0.01$. Data are represented as mean ± SEM.

overall shape of each insulin secretory trace, with the macroperifusion showing a "saw-tooth" pattern (Supplemental Figure 4H) while the microperifusion had a more progressive increase (Supplemental Figure 4I). Using this approach, we found that differences in the insulin secretory profiles were primarily due to the different fluid dynamics and experimental parameters between the two perifusion systems, especially the experimental time for each stimulus and the flow rate. Overall, this analysis demonstrates how perifusion parameters can affect insulin secretory pattern and indicates the strength of using complementary approaches. It also emphasizes the importance of validating new microperifusion devices (46, 47) by comparing these with macroperifusion systems that have been used for many years by many laboratories.

When G_q signaling was activated with CNO, we again saw a transient stimulation of insulin secretion at low glucose followed by relative inhibition through the glucose ramp, while glucagon secretion from α cells was stimulated throughout the entire perifusion, independently of glucose concentration (Figure 5, C, D, and G–J). Furthermore, the Ca^{2+} dynamics in response to G_q activation were consistent with the insulin secretory trace showing a rapid but short-lived increase in intracellular Ca^{2+}. Interestingly, the Ca^{2+} signal remained elevated above baseline but did not significantly increase with rising glucose (Figure 5, B, E, and F). This indicates that the dual effects of G_q signaling on insulin secretion in β cells are largely mediated by changes in intracellular Ca^{2+} levels.

Discussion

The 3D multicellular human islet architecture, while essential for islet cell function presents experimental challenges for mechanistic studies of intracellular signaling pathways. Using primary human islets, we developed a pseudoislet system that resembles native human islets in morphology, cellular composition, cell identity, and dynamic insulin and glucagon secretion. This system allows for efficient virally mediated genetic manipulation in almost all cells in the pseudoislet. To evaluate the coordination between intracellular signals and islet hormone secretion, we developed an integrated system consisting of pseudoislets and a microfluidic device that enables studies of islet intracellular signaling using genetically encoded biosensors in conjunction with hormone secretion. Furthermore, we used this integrated approach to define aspects of human islet biology by investigating GPCR signaling pathways using DREADDs and a calcium biosensor.

Despite α and β cells both being excitable secretory cells and sharing many common developmental and signaling components, this experimental approach allowed us to demonstrate similar and distinct responses to activation of GPCR signaling pathways, highlighting the uniqueness in each cell's molecular machinery. The activation of G_i signaling was inhibitory in β and α cells, resulting in reduced insulin and glucagon secretion, respectively, and showed a more substantial affect in β cells, where this signaling blunted insulin response to both a glucose ramp and to KCl-mediated depolarization. Interestingly, direct KCl depolarization was not sufficient to overcome these inhibitory effects in either β or α cells, suggesting that reduced cAMP via the inhibition of adenylyl cyclase, in addition to cAMP-independent pathways (48), plays a role in both insulin and glucagon secretion. These results align well with those of recent studies in β cells, suggesting that cAMP tone is crucial for insulin secretion, and observations in α cells highlighting cAMP as a key mediator of glucagon secretion (13, 17, 19, 49).

There were major differences in response to activation of G_q signaling in β cells compared with α cells. In α cells, the activated G_q signaling elicited a robust and sustained increase in glucagon secretion in the presence of a glucose ramp and potassium chloride. In contrast, G_q signaling in β cells had a transient stimulatory effect in low glucose and then inhibitory effects on both insulin and intracellular Ca^{2+} levels, with sustained activation during glucose ramp. Interestingly, previous studies of acetylcholine signaling have also reported dual effects on Ca^{2+} dynamics in β cells depending on the length of stimulation (50). This signaling was thought to be mediated through the muscarinic acetylcholine receptor M_3 (from which the hM3Dq DREADD is based). Overall, these results suggest a negative feedback or protective mechanism that prevents sustained insulin release from β cells in response to G_q signaling that is not active in α cells under similar circumstances.

There are limitations and caveats to the current study. First, our approach resulted in DREADD expression in all cell types. Although we can distinguish the effects on islet α and β cells through their distinct hormone secretion, it is possible that complex paracrine signaling contributes to the results described here. Future modifications of this system could incorporate cell-specific promoters to target a particular islet cell type. Second, the DREADDs are likely expressed at higher levels than endogenous GPCRs. To mitigate this, we used the appropriate DREADD-expressing pseudoislets as our controls and were encouraged to see normal secretory responses in these control pseudoislets. Third, while there is some concern that CNO can be reverse metabolized in vivo into clozapine, which could potentially have off-target effects (51), this is unlikely in our in vitro system. We also verified that CNO had no effect on mCherry-expressing pseudoislets, making it unlikely that CNO itself is competitively inhibiting endogenous receptors in human islets. Fourth, we used a CNO concentration of 10 μM for all of our experiments, a standard concentration used for in vitro assays (16, 52), but it is possible that islet cells may show dose-dependent effects. Finally, this is an in vitro study focused on acute functional effects of these pathways on human islets, and chronic in vivo studies of these pathways may show different results. For example, in mouse β cells, chronic in vivo activation of G_q pathways using the DREADD system lead to an increase in β cell function and mass (53) while inhibition of G_i signaling with β cell–specific pertussis toxin expression affected only function (54). Future work could involve transplantation of DREADD-expressing pseudoislets into immunodeficient mice to study the effect of activating these pathways on human islets in vivo (55).

Overall, these findings demonstrate the utility of the pseudoislet system for its ability to manipulate human islets. Other approaches include inducible pluripotent stem cells that allow similar genetic manipulation. However, it is unclear if these approaches create entirely normal human islet cells. We show in this system that α and β cells in pseudoislets maintain their fully differentiated state as well as their dynamic responsiveness to glucose and other stimuli. Additionally, this approach allows for the study of all islet cells within the context of

other cell types and 3D assembly. While our data suggest that breaking down and rebuilding the islet does not impair paracrine interactions, this could be further evaluated by looking at secretion in response to factors that exclusively rely on paracrine interactions such as ghrelin or certain amino acids (17, 56, 57).

Ultimately, the integration of the pseudoislet approach with a microfluidic perifusion system and live-cell imaging provides a powerful experimental platform to gain insight into human islet biology and the mechanisms controlling regulated islet hormone secretion, which currently limit the development of novel therapeutic approaches. Here, we focus on virally mediated gene expression to alter signaling pathways, but this system could be adapted to accommodate technologies such as CRISPR. Furthermore, after islet dispersion into single cells, techniques to purify live-cell populations such as FACS with cell surface antibodies (41, 58) could be incorporated to allow manipulation of the pseudoislet cellular composition as well as cell-specific gene manipulation. Combined with accurate cell-specific targeting, this approach would allow the measurement of intracellular dynamics at the individual cell level and distinguish intracellular responses of islet endocrine cells to stimuli.

Methods

Human islet isolation. Human islets (n = 24 preparations, Supplemental Table 1) were obtained through partnerships with the IIDP (https://iidp.coh.org/), Alberta Diabetes Institute IsletCore (https://www.epicore.ualberta.ca/IsletCore/), and Human Pancreas Analysis Program (https://hpap.pmacs.upenn.edu/) or isolated at the Institute of Cellular Therapeutics of the Allegheny Health Network. Assessment of human islet function was performed by islet macroperifusion assay on the day of arrival, as previously described (42). Primary human islets were cultured in CMRL 1066 (MediaTech, 15-110-CV) media (5.5 mM glucose, 10% FBS [MilliporeSigma, 12306C], 1% Penicillin/Streptomycin [Gibco, 15140-122], 2 mM L-glutamine [Gibco, 25030-081]) in 5% CO_2 at 37°C for <24 hours before beginning studies.

This study used data from the Organ Procurement and Transplantation Network (OPTN) that was in part compiled from the data hub accessible to IIDP-affiliated investigators through the IIDP portal (https://iidp.coh.org/secure/isletavail). The OPTN data system includes data on all donors, wait-listed candidates, and transplant recipients in the US, submitted by the members of OPTN. The Health Resources and Services Administration of the US Department of Health and Human Services provides oversight of the activities of the OPTN contractor. The data reported here have been supplied by UNOS as the contractor for OPTN. The interpretation and reporting of these data are the responsibility of the author(s) and in no way should be seen as an official policy of or interpretation by the OPTN or the US government.

Pseudoislet formation. See Vanderbilt Pseudoislet Protocol in Supplemental Information for the detailed pseudoislet formation protocol. Briefly, human islets were handpicked to purity and then dispersed with HyClone trypsin (Thermo Scientific). Islet cells were counted and then seeded at 2000 cells per well in CellCarrier Spheroid Ultra-low attachment microplates (PerkinElmer) or 2500 cells per drop in GravityPLUS Hanging Drop System (InSphero) in enriched Vanderbilt pseudoislet media (see Vanderbilt Pseudoislet Protocol in Supplemental Information for detailed protocol). Cells were allowed to reaggregate for 6 days before being harvested and studied.

Immunohistochemical analysis. Immunohistochemical analysis of islets was performed by whole mount or on 8-μm cryosections of islets embedded in collagen gels as previously described (3, 21). Primary antibodies against all antigens and their working dilutions are listed in Supplemental Table 2. Apoptosis was assessed by TUNEL (MilliporeSigma, S7165) following the manufacturer's instructions. Digital images were acquired with a Zeiss LSM 880 or LSM 510 laser-scanning confocal microscope (Zeiss Microscopy Ltd) or ScanScope FL (Aperio/Leica Biosystems). Images were analyzed using HALO Image Analysis Software (Indica Labs) or MetaMorph v7.1 (Molecular Devices LLC).

Adenovirus. Adenoviral vectors CMV-mCherry (VB180905-1046uck), CMV-hM4Di-mCherry (VB180904-1144bbp), and CMV-hM3Dq-mCherry (VB160707-1172csx) were constructed by VectorBuilder Inc., and adenovirus was prepared, amplified, and purified by the Human Islet and Adenovirus Core of the Einstein-Sinai Diabetes Research Center or Welgen Inc. Titers were determined by plaque assay. Ad-CMV-GCaMP6f was purchased from Vector Biolabs (catalog 1910). Dispersed human islets were incubated with adenovirus at a multiplicity of infection of 500 for 2 hours in Vanderbilt pseudoislet media before being spun, washed, and plated.

Assessment of islet function in vitro by static incubation. Pseudoislets (10–20 IEQs/well) were placed in 2 mL DMEM (media, 2 mM glucose) of a 12-well plate (351143, Corning) and allowed to equilibrate for 30 minutes and then were transferred to media containing the stimuli of interest for 40 minutes.

Media from this incubation was assessed for insulin and glucagon by radioimmunoassay (insulin, RI-13K, MilliporeSigma; glucagon, GL-32K, MilliporeSigma; somatostatin, RK-060-03, Phoenix Pharmaceuticals) as previously reported (3).

Assessment of islet function by macroperifusion. Function of native islets and pseudoislets was studied in a dynamic cell perifusion system at a perifusate flow rate of 1 mL/min as described previously (3, 42) using approximately 250 IEQs/chamber. The effluent was collected at 3-minute intervals using an automatic fraction collector. Insulin and glucagon concentrations in each perifusion fraction and islet extracts were measured by radioimmunoassay (insulin, RI-13K; glucagon, GL-32K, MilliporeSigma).

Microperifusion platform. The microperifusion platform (Figure 5 and Supplemental Figure 4) is based on a previously published microfluidic device with modifications (43). Design modifications were incorporated using SolidWorks 2018 3D computer-aided design (CAD) software. Microfluidic devices were machined, according to the CAD models, using a computer numerical controlled milling machine (MDX-540, Roland) from poly(methyl methacrylate) workpieces. To reduce the optical working distance, through holes were milled into the culture wells and a no. 1.5 glass coverslip was bonded to the bottom component of the microfluidic device using a silicone adhesive (7615A21, McMaster-Carr). Custom gaskets were fabricated using a 2-part silicone epoxy (Duraseal 1533, Cotronics Corp.) and bonded into the top component of the device using a specialized polyester adhesive (PS-1340, Polymer Science). The 2 components of the microfluidic device (Supplemental Figure 4A) were assembled in a commercially available device holder (Fluidic Connect PRO with 4515 Inserts, Micronit Microfluidics), which creates a sealed system and introduces fluidic connections to a peristaltic pump (P720, Instech) though 0.01-inch FEP tubing (IDEX, 1527L) and a low-volume bubble trap (Omnifit, 006BT) placed in the fluid line just before the device inlet to prevent bubbles from entering the system (see Supplemental Figure 4B for microperifusion assembly).

Assessment of pseudoislets by microperifusion. The microperifusion apparatus was contained in a temperature-controlled incubator (37°C) fitted to a Zeiss LSM 880 laser-scanning confocal microscope (Zeiss Microscopy Ltd) (Supplemental Figure 4B). Pseudoislets (~25 IEQs/chamber) were loaded in a prewetted well, imaged with a stereomicroscope to determine loaded IEQ, and perifused at 100 μL/min flow rate with Krebs-Ringer buffer containing 125 mM NaCl, 5.9 mM KCl, 2.56 mM $CaCl_2$, 1 mM $MgCl_2$, 25 mM HEPES, 0.1% BSA, pH 7.4, at 37°C. Perifusion fractions were collected at 2-minute intervals following a 20-minute equilibration period in 2 mM glucose using a fraction collector (model 2110, Bio-Rad) and analyzed for insulin and glucagon concentration by RIA (insulin, RI-13K; glucagon, GL-32K, MilliporeSigma). GCaMP6f biosensor was excited at 488 nm and fluorescence emission detected at 493–574 nm. Images were acquired at 15-μm depth every 5 seconds using a ×20/0.80 Plan-Apochromat objective. Image analysis was performed with MetaMorph v7.1 software (Molecular Devices). Pseudoislets in the field of view (3–7 pseudoislets/field) were annotated using the region-of-interest tool. The GCaMP6f fluorescence intensity recorded for each time point was measured across annotated pseudoislet regions and normalized to the baseline fluorescence intensity acquired over the 60 seconds in 2 mM glucose before stimulation. The calcium, insulin, and glucagon traces were averaged from 5 microperifusion experiments from 3 independent donors.

Fluid dynamics and mass transport modeling. 2D finite element method (FEM) models, which incorporate fluid dynamics, mass transport, and islet physiology, were developed for the macroperifusion and microperifusion platforms and implemented in COMSOL Multiphysics Modeling Software (release version 5.0). Fluid dynamics were governed by the Navier-Stokes equation for incompressible Newtonian fluid flow. Convective and diffusive transport of oxygen, glucose, and insulin were governed by the generic equation for transport of a diluted species in the chemical species transport module. Islet physiology was based on Hill (generalized Michaelis-Menten) kinetics using local concentrations of glucose and oxygen, as previously described (44, 45). The geometry of the macroperifusion platform was modeled as the 2D cross section of a cylindrical tube with fluid flowing from bottom to top (Supplemental Figure 4D). The geometry of the microperifusion platform was modeled as a 2D cross section of the microfluidic device with fluid flow from left to right (Supplemental Figure 4E). In both the macroperifusion and microperifusion models, 5 islets with a diameter of 150 μm (5 IEQs) were placed in the flow path. FEM models were solved as a time-dependent problem, allowing for intermediate time steps that corresponding with fraction collection time during macroperifusion and microperifusion. A list of the parameters used in the computational models is provided in Supplemental Table 3.

Statistics. Data are expressed as mean ± SEM. A *P* value of less than 0.05 was considered significant. Analyses of area under the curve and statistical comparisons (Mann-Whitney test, Wilcoxon matched-pairs signed-rank test, and 1- and 2-way ANOVA) were performed using Prism v8 software (GraphPad). Statistical details of experiments are described in the figure legends and the Results.

Study approval. The Vanderbilt University Institutional Review Board does not classify deidentified human pancreatic specimens as human subject research.

Author contributions

JTW, RH, HAN, MI, JRL, AA, MB, and ACP conceived and designed the experiments. JTW, RH, HAN, GP, RA, CR, DCS, MI, PW, AGO, RB, and MB performed experiments or analyzed the data and interpreted results. JTW, MB, and ACP wrote the manuscript. All authors reviewed, edited, and approved the final version.

Acknowledgments

We thank the organ donors and their families for their invaluable donation and the International Institute for Advancement of Medicine, Organ Procurement Organizations, National Disease Research Exchange, and the Alberta Diabetes Institute IsletCore for their partnership in studies of human pancreatic tissue for research. This study used human pancreatic islets that were provided by the National Institute of Diabetes and Digestive and Kidney Diseases–funded IIDP at the City of Hope (NIH grant 2UC4 DK098085). Experiments were performed in part through the use of the Vanderbilt Cell Imaging Shared Resource (supported by NIH grants CA68485, DK20593, DK58404, DK59637 and EY08126). This research was performed using resources and/or funding provided by the National Institute of Diabetes and Digestive and Kidney Diseases–supported Human Islet Research Network (RRID:SCR_014393; https://hirnetwork.org; UC4 DK104211, DK108120, DK112232, DK120456, DK122638, DK104208), by NIH grants DK106755, DK117147, DK94199, T32GM007347, F30DK118830, F30DK112630, F31DK118860, F30AA027126, P30DK020541, and DK20593; by grants from JDRF (2-SRA-2019-699-S-B); by The Leona M. and Harry B. Helmsley Charitable Trust, and by the Department of Veterans Affairs (BX000666).

Address correspondence to: Marcela Brissova or Alvin C. Powers, Vanderbilt University, 7465 MRB IV, 2213 Garland Avenue, Nashville, Tennessee 37232-0475, USA. Phone: 615.936.1729; Email: marcela.brissova@vanderbilt.edu (MB). Phone: 615.936.7678; Email: al.powers@vumc.org (ACP). Or to: Ashutosh Agarwal, University of Miami, #475, 1951 NW 7th Avenue, Miami, Florida 33136, USA. Phone: 305.243.8925; Email: a.agarwal2@miami.edu.

1. Chen C, Cohrs CM, Stertmann J, Bozsak R, Speier S. Human beta cell mass and function in diabetes: Recent advances in knowledge and technologies to understand disease pathogenesis. *Mol Metab*. 2017;6(9):943–957.
2. Halban PA, et al. β-Cell failure in type 2 diabetes: postulated mechanisms and prospects for prevention and treatment. *Diabetes Care*. 2014;37(6):1751–1758.
3. Brissova M, et al. α Cell function and gene expression are compromised in type 1 diabetes. *Cell Rep*. 2018;22(10):2667–2676.
4. Lu M, Li C. Nutrient sensing in pancreatic islets: lessons from congenital hyperinsulinism and monogenic diabetes. *Ann N Y Acad Sci*. 2018;1411(1):65–82.
5. Naylor RN, Greeley SA, Bell GI, Philipson LH. Genetics and pathophysiology of neonatal diabetes mellitus. *J Diabetes Investig*. 2011;2(3):158–169.
6. Hart NJ, et al. Cystic fibrosis-related diabetes is caused by islet loss and inflammation. *JCI Insight*. 2018;3(8):98240.
7. Haliyur R, et al. Human islets expressing HNF1A variant have defective β cell transcriptional regulatory networks. *J Clin Invest*. 2019;129(1):246–251.
8. Gloyn AL, et al. Activating mutations in the gene encoding the ATP-sensitive potassium-channel subunit Kir6.2 and permanent neonatal diabetes. *N Engl J Med*. 2004;350(18):1838–1849.
9. Talchai C, Xuan S, Lin HV, Sussel L, Accili D. Pancreatic β cell dedifferentiation as a mechanism of diabetic β cell failure. *Cell*. 2012;150(6):1223–1234.
10. Cnop M, Welsh N, Jonas JC, Jörns A, Lenzen S, Eizirik DL. Mechanisms of pancreatic beta-cell death in type 1 and type 2 diabetes: many differences, few similarities. *Diabetes*. 2005;54 Suppl 2:S97–107.
11. Unger RH, Cherrington AD. Glucagonocentric restructuring of diabetes: a pathophysiologic and therapeutic makeover. *J Clin Invest*. 2012;122(1):4–12.
12. Tokarz VL, MacDonald PE, Klip A. The cell biology of systemic insulin function. *J Cell Biol*. 2018;217(7):2273–2289.
13. Yu Q, Shuai H, Ahooghalandari P, Gylfe E, Tengholm A. Glucose controls glucagon secretion by directly modulating cAMP in

alpha cells. *Diabetologia*. 2019;62(7):1212–1224.
14. Gylfe E, Gilon P. Glucose regulation of glucagon secretion. *Diabetes Res Clin Pract*. 2014;103(1):1–10.
15. Hughes JW, Ustione A, Lavagnino Z, Piston DW. Regulation of islet glucagon secretion: Beyond calcium. *Diabetes Obes Metab*. 2018;20 Suppl 2:127–136.
16. Zhu L, et al. Intra-islet glucagon signaling is critical for maintaining glucose homeostasis. *JCI Insight*. 2019;5:127994.
17. Capozzi ME, et al. β Cell tone is defined by proglucagon peptides through cAMP signaling. *JCI Insight*. 2019;4(5):126742.
18. Svendsen B, et al. Insulin secretion depends on intra-islet glucagon signaling. *Cell Rep*. 2018;25(5):1127–1134.e2.
19. Elliott AD, Ustione A, Piston DW. Somatostatin and insulin mediate glucose-inhibited glucagon secretion in the pancreatic α-cell by lowering cAMP. *Am J Physiol Endocrinol Metab*. 2015;308(2):E130–E143.
20. Unger RH, Orci L. Paracrinology of islets and the paracrinopathy of diabetes. *Proc Natl Acad Sci USA*. 2010;107(37):16009–16012.
21. Brissova M, et al. Assessment of human pancreatic islet architecture and composition by laser scanning confocal microscopy. *J Histochem Cytochem*. 2005;53(9):1087–1097.
22. Dai C, et al. Islet-enriched gene expression and glucose-induced insulin secretion in human and mouse islets. *Diabetologia*. 2012;55(3):707–718.
23. Cabrera O, Berman DM, Kenyon NS, Ricordi C, Berggren PO, Caicedo A. The unique cytoarchitecture of human pancreatic islets has implications for islet cell function. *Proc Natl Acad Sci USA*. 2006;103(7):2334–2339.
24. Rodriguez-Diaz R, et al. Paracrine interactions within the pancreatic islet determine the glycemic set point. *Cell Metab*. 2018;27(3):549–558.e4.
25. Yu Y, et al. Bioengineered human pseudoislets form efficiently from donated tissue, compare favourably with native islets in vitro and restore normoglycaemia in mice. *Diabetologia*. 2018;61(9):2016–2029.
26. Peiris H, et al. Discovering human diabetes-risk gene function with genetics and physiological assays. *Nat Commun*. 2018;9(1):3855.
27. Arda HE, et al. Age-dependent pancreatic gene regulation reveals mechanisms governing human β cell function. *Cell Metab*. 2016;23(5):909–920.
28. Hilderink J, et al. Controlled aggregation of primary human pancreatic islet cells leads to glucose-responsive pseudoislets comparable to native islets. *J Cell Mol Med*. 2015;19(8):1836–1846.
29. Furuyama K, et al. Diabetes relief in mice by glucose-sensing insulin-secreting human α-cells. *Nature*. 2019;567(7746):43–48.
30. Zuellig RA, et al. Improved physiological properties of gravity-enforced reassembled rat and human pancreatic pseudo-islets. *J Tissue Eng Regen Med*. 2017;11(1):109–120.
31. Foty R. A simple hanging drop cell culture protocol for generation of 3D spheroids. *J Vis Exp*. 2011;(51):2720.
32. Ahrén B. Islet G protein-coupled receptors as potential targets for treatment of type 2 diabetes. *Nat Rev Drug Discov*. 2009;8(5):369–385.
33. Persaud SJ. Islet G-protein coupled receptors: therapeutic potential for diabetes. *Curr Opin Pharmacol*. 2017;37:24–28.
34. Weis WI, Kobilka BK. The molecular basis of G protein-coupled receptor activation. *Annu Rev Biochem*. 2018;87:897–919.
35. Foord SM, et al. International Union of Pharmacology. XLVI. G protein-coupled receptor list. *Pharmacol Rev*. 2005;57(2):279–288.
36. Hauser AS, Attwood MM, Rask-Andersen M, Schiöth HB, Gloriam DE. Trends in GPCR drug discovery: new agents, targets and indications. *Nat Rev Drug Discov*. 2017;16(12):829–842.
37. Armbruster BN, Li X, Pausch MH, Herlitze S, Roth BL. Evolving the lock to fit the key to create a family of G protein-coupled receptors potently activated by an inert ligand. *Proc Natl Acad Sci USA*. 2007;104(12):5163–5168.
38. Wess J. Use of designer Gprotein-coupled receptors to dissect metabolic Pathways. *Trends Endocrinol Metab*. 2016;27(9):600–603.
39. Roth BL. DREADDs for neuroscientists. *Neuron*. 2016;89(4):683–694.
40. Guettier JM, et al. A chemical-genetic approach to study G protein regulation of beta cell function in vivo. *Proc Natl Acad Sci USA*. 2009;106(45):19197–19202.
41. Saunders DC, et al. Ectonucleoside triphosphate diphosphohydrolase-3 antibody targets adult human pancreatic β cells for in vitro and in vivo analysis. *Cell Metab*. 2019;29(3):745–754.e4.
42. Kayton NS, et al. Human islet preparations distributed for research exhibit a variety of insulin-secretory profiles. *Am J Physiol Endocrinol Metab*. 2015;308(7):E592–E602.
43. Lenguito G, et al. Resealable, optically accessible, PDMS-free fluidic platform for ex vivo interrogation of pancreatic islets. *Lab Chip*. 2017;17(5):772–781.
44. Buchwald P, Tamayo-Garcia A, Manzoli V, Tomei AA, Stabler CL. Glucose-stimulated insulin release: Parallel perifusion studies of free and hydrogel encapsulated human pancreatic islets. *Biotechnol Bioeng*. 2018;115(1):232–245.
45. Buchwald P. A local glucose-and oxygen concentration-based insulin secretion model for pancreatic islets. *Theor Biol Med Model*. 2011;8:20.
46. Wang Y, et al. Application of microfluidic technology to pancreatic islet research: first decade of endeavor. *Bioanalysis*. 2010;2(10):1729–1744.
47. Jun Y, et al. In vivo-mimicking microfluidic perfusion culture of pancreatic islet spheroids. *Sci Adv*. 2019;5(11):eaax4520.
48. Schwetz TA, Ustione A, Piston DW. Neuropeptide Y and somatostatin inhibit insulin secretion through different mechanisms. *Am J Physiol Endocrinol Metab*. 2013;304(2):E211–E221.
49. Tengholm A, Gylfe E. cAMP signalling in insulin and glucagon secretion. *Diabetes Obes Metab*. 2017;19 Suppl 1:42–53.
50. Gilon P, Nenquin M, Henquin JC. Muscarinic stimulation exerts both stimulatory and inhibitory effects on the concentration of cytoplasmic Ca2+ in the electrically excitable pancreatic B-cell. *Biochem J*. 1995;311(Pt 1):259–267.
51. Gomez JL, et al. Chemogenetics revealed: DREADD occupancy and activation via converted clozapine. *Science*. 2017;357(6350):503–507.
52. Smith KS, Bucci DJ, Luikart BW, Mahler SV. DREADDS: Use and application in behavioral neuroscience. *Behav Neurosci*. 2016;130(2):137–155.
53. Jain S, Ruiz de Azua I, Lu H, White MF, Guettier JM, Wess J. Chronic activation of a designer G(q)-coupled receptor improves β cell function. *J Clin Invest*. 2013;123(4):1750–1762.
54. Regard JB, et al. Probing cell type-specific functions of Gi in vivo identifies GPCR regulators of insulin secretion. *J Clin Invest*.

2007;117(12):4034–4043.
55. Dai C, et al. Age-dependent human β cell proliferation induced by glucagon-like peptide 1 and calcineurin signaling. *J Clin Invest*. 2017;127(10):3835–3844.
56. Gray SM, et al. Intraislet ghrelin signaling does not regulate insulin secretion from adult mice. *Diabetes*. 2019;68(9):1795–1805.
57. DiGruccio MR, et al. Comprehensive alpha, beta and delta cell transcriptomes reveal that ghrelin selectively activates delta cells and promotes somatostatin release from pancreatic islets. *Mol Metab*. 2016;5(7):449–458.
58. Dorrell C, et al. Isolation of major pancreatic cell types and long-term culture-initiating cells using novel human surface markers. *Stem Cell Res*. 2008;1(3):183–194.